Surface Science 653 (2016) 169–180

Contents lists available at ScienceDirect

Surface Science

journal homepage: www.elsevier.com/locate/susc

Simulation and fitting of complex reaction network TPR: The key is the objective function☆

Aditya Savara

Chemical Sciences Division, Oak Ridge National Lab, 1 Bethel Valley Road, Oak Ridge, TN 37830, United States

ARTICLE INFO

Article history:
Received 28 March 2016
Received in revised form 27 June 2016
Accepted 5 July 2016
Available online 7 July 2016

Keywords:
Temperature programmed desorption
Temperature programmed reaction
Microkinetics
Transient kinetics
Parameter optimization

ABSTRACT

A method has been developed for finding improved fits during simulation and fitting of data from complex reaction network temperature programmed reactions (CRN-TPR). It was found that simulation and fitting of CRN-TPR presents additional challenges relative to simulation and fitting of simpler TPR systems. The method used here can enable checking the plausibility of proposed chemical mechanisms and kinetic models. The most important finding was that when choosing an objective function, use of an objective function that is based on integrated production provides more utility in finding improved fits when compared to an objective function based on the rate of production. The response surface produced by using the integrated production is monotonic, suppresses effects from experimental noise, requires fewer points to capture the response behavior, and can be simulated numerically with smaller errors. For CRN-TPR, there is increased importance (relative to simple reaction network TPR) in resolving of peaks prior to fitting, as well as from weighting of experimental data points. Using an implicit ordinary differential equation solver was found to be inadequate for simulating CRN-TPR. The method employed here was capable of attaining improved fits in simulation and fitting of CRN-TPR when starting with a postulated mechanism and physically realistic initial guesses for the kinetic parameters.

1. Introduction

Temperature programmed reaction (TPR) experiments (including temperature programmed desorption or decomposition) are used to gain insight into the kinetics and mechanisms for reactions on surfaces. There has been relatively little work in simulating and fitting the chemical kinetics of complex reaction networks (CRNs) in the context of TPR. A methodology is presented here for finding improved fits in simulation and fitting of complex reaction network temperature programmed reactions (CRN-TPR), provided a reaction mechanism and initial guesses for kinetic parameters. During this work, challenges were encountered in the simulation and fitting of the kinetics CRN-TPR that are (in some cases) different from simulation and fitting of simple reaction network TPR, and attention is drawn to these differences.

A key issue is choosing an effective objective function during the parameter optimization for simulation and fitting, to guide improvement of the parameters used during fitting. In general, the output from an objective function is used during fitting/optimization to gauge how well a proposed set of model parameters can reproduce all of the experimental results, and thus to gauge whether the fit has been improved when parameters are changed. Typically, the lower the value of the objective function is for a given set of parameters as input, the better the fit is considered to be. For example, one common choice for the objective function is the sum of squared residuals (SSR) between the simulated data points and the experimental data points. After choosing an objective function, such as the SSR, the parameters are varied with the intent of finding as low (or high) a value of the objective function as possible. Here, we found that a good objective function for simulation and fitting of CRN-TPR is a weighted sum of squared residuals based on the integrated quantities of the products formed (or, more generally, integrated extent of reaction). Each dependent variable (such as concentration or other output of the simulation) can be called a "response variable", and the objective function can be dependent on multiple responses. In the example shown in this work, the objective function is based on the quantities of production of several gas phase species.

It is instructive to consider the importance of using gradient based optimization, as well as the limitations. Each simulation here takes >1 s of runtime on a desktop computer. This means that testing a 10 × 10 grid of values for 2 parameters (i.e., 10 values for each parameter) takes > 10^2 seconds. For 5 parameters, a 10^n value

☆ Notice: This manuscript has been authored by UT-Battelle, LLC under Contract No. DE-AC05-00OR22725 with the U.S. Department of Energy. The United States Government retains and the publisher, by accepting the article for publication, acknowledges that the United States Government retains a non-exclusive, paid-up, irrevocable, world-wide license to publish or reproduce the published form of this manuscript, or allow others to do so, for United States Government purposes. The Department of Energy will provide public access to these results of federally sponsored research in accordance with the DOE Public Access Plan (http://energy.gov/downloads/doe-public-access-plan).

E-mail address: savaraa@ornl.gov.

http://dx.doi.org/10.1016/j.susc.2016.07.001
0039-6028/

multidimensional grid would take >1 day, for 7 parameters >1 year, for 17 parameters it is greater than the lifetime of the universe. For 10 parameters, the problem already becomes prohibitive even with supercomputers. Over 10 parameters were varied in this study. For this reason, gradient optimization was required, and this requires a well behaved objective function surface: if the objective function has too many local minima or discontinuities, the gradient optimization will not be successful. For problems with many parameters, gradient optimization is good at finding improved fits *near* the optimum without necessarily finding the true optimum. Thus, an improved fit can be expected, but not a perfect fit. When trying to show the plausibility of a reaction mechanism and kinetic model in CRN-TPR, a perfect fit is not required: merely the production of the correct species in the correct temperature range.

To our knowledge, no previous work has been published on finding improved fits during simulation and fitting of CRN-TPR. Thus, this work is intended to lay down initial guidance for continued progress. For some context, the methods in this work may be applied to systems with an arbitrary number of reactions and an arbitrary number of species (in this example, a system with >20 reactions and >20 species), including cases with reaction pathways that include loops. We are not aware of similar work for temperature programmed reaction conditions, in the context of elucidating mechanisms. In comparison, one of the best softwares available for complex thermal analysis kinetics by simulation and fitting is the Advanced Software by Netzch Instruments, and as of 2015 the Netzch software allows for 78 different models which all have ≤6 reaction steps, and ≤7 species per reaction, and only linear reaction mechanisms (i.e., no loops). Thus, the type of problem being considered in this work is beyond what is currently available in widely distributed software packages. In this type of problem, it is difficult to find *any* good fit due to the vast parameter space available (this is not the type of problem where it is easy to minimize the residuals). The present manuscript documents a path that was followed for achieving an improved fit when simulating the kinetics of a CRN-TPR experiment [1], and the path followed was sufficient for showing the plausibility of a reaction mechanism when using physically realistic parameters, enabling guidelines to be provided for further progress in simulation and fitting of CRN-TPR.

1.1. Background

"Microkinetic modeling" refers to simulation/characterization in which each elementary chemical reaction step [2] is included in the model [3–7]. Sophisticated microkinetic numerical modeling of CRNs on surfaces has been achieved for steady-state conditions [8–13]. In contrast, microkinetic numerical modeling of CRNs on surfaces under transient conditions – particularly temperature programmed conditions [14–16] – has been uncommon and generally un-sophisticated [14–25]. Some disparate aspects of the methodology needed are mature: numerical simulation of temperature programmed reactions [26], kinetic parameter estimation from temperature programmed reactions [21], parameter estimation/optimization for ordinary differential equation-based transient kinetics [27–30], improved global optimization of parameters for ordinary differential equations [19], and the difficulties in assessing the correctness of a complex model for transient kinetics [28,31–33]. In this work, we provide a step forward for simulation and fitting of CRNs under transient conditions in which the temperature is varied widely. The present work is written in the context of reactions on surfaces, but these methods may be used for other CRN-TPR as well.

One of the motivations for using temperature programmed reaction conditions is that these conditions can have advantages over isothermal reaction conditions when gaining initial estimates for activation energies. When an Arrhenius-like expression can be assumed for rate constants, temperature programmed reaction can provide initial estimates for activation energies with fewer experiments than isothermal experiments [34], particularly when there is a coverage (or concentration) dependence of kinetic parameters. We and others have shown previously that for catalytic reactions on surfaces, a coverage dependence with a change in the activation energy on the order of 10% can result in dramatic changes in observed steady-state reaction orders – as dramatic as a change in mechanism [9,10,35–39]. In this context, temperature programmed desorption shows a significant but less dramatic change in temperature position when the activation energy changes on the order of 10% as a function of coverage [40–42]. Another advantage of TPR is that multiple product peaks may appear across success temperature ranges, particularly when stable intermediates are formed, which can aid in elucidating reaction mechanisms [43,44]. Thus, for many systems, temperature programmed reaction experiments can reveal more mechanistic information than isothermal experiments [34], and serve as a useful method for establishing a reaction mechanism and extracting estimates of activation energies [34,43,44].

The reaction model which will be simulated in this work begins with an initial state with molecules absorbed on a surface: methanol on $CeO_2(111)$. The surface is subsequently subjected to a temperature ramp, whereupon surface reactions (including desorption) occur, and the gas phase products evolved are detected by mass spectrometry. The data used is experimental data from reference [1]. The CRN-TPR simulation involves 6 gas-phase products and >20 distinct possible chemical species (i.e., >20 state equations), with an analogous quantity of reactions, and over 50 parameters. The mechanism involves long-lived intermediates on the surface and the selectivity towards the various products occurs in different temperature ranges (this presents additional challenges from stiffness). The selectivity is sensitive to multiple kinetic parameters in ways that are not easy to predict ahead of time. We are not aware of any study applying simulation and fitting to a reaction network of comparable complexity with the aim of establishing a reaction mechanism. Here, a method is presented that seems to be adequate and general, including details on the data treatment and the choice of objective function for simulation and fitting of CRN-TPR. Some forward-looking discussion of applying parameter optimization techniques to the resulting multi-dimensional objective function surface is also provided.

1.2. Motivation for numerical modeling

Although peak shape and linearization methods exist (as described in Section S.·VII of the Supporting information), numerical simulations may be the only practical method for fitting of CRN-TPR, and others have noted that numerical simulations [45,46] have advantages for TPR of even simple reaction networks. In the context of CRN-TPR, numerical simulations have several strengths: 1) numerical simulations enable varied functional forms for the rate equation to be adopted/tested with relative ease, 2) numerical simulations can accurately describe complex mechanisms, even with concentration dependent terms and coupled kinetic equations, 3) fewer a priori assumptions about the chemical system need to be made for numerical simulations, relative to peak shape methods (alternative mechanisms can be tested without a new derivation).

Although numerical simulations can interrogate various multi-step mechanisms and various functional forms for rate equations with relative ease, drawing mechanistic/chemical conclusions requires having both the correct mechanism and the correct functional form of the rate equation(s), as noted in the analysis of the ICTAC kinetics project-data [47–50] and elsewhere (further discussion on the role of simulation and fitting is provided in Section S.·VI of the Supporting information). How to elucidate a mechanism [51] is beyond the scope of this work: this work focuses on how to treat the data and create an objective function that enables achieving a reasonable fit when given a proposed mechanism and physically meaningful initial guesses for parameters. In this work, ordinary differential equations were used for the numerical simulations. An alternative method for performing numerical

simulations is to use kinetic Monte Carlo methods, which is noted in Section S.·IV of the Supporting information.

2. Steps in simulation and fitting of experimental data

Simulation and fitting of experimental chemical kinetics data to obtain kinetic parameters and chemico-physical insights consists of several sequential steps [21,27,32,33,52]. Here, the steps will be delineated as follows: 1) model formulation (reaction network and rate equations), 2) initial guesses for parameters, 3) transformation of experimental data, 4) simulation using initial guesses, 5) parameter estimation/optimization and refinement of the model, 6) interrogation of the simulated output for chemico-physical insights. The above process may be iterative, and may include design of additional experiments.

Here, the word "model" refers to the set of chemical species which are defined as part of the reaction network (including surface sites) as well as the reactions (rate equations) which connect the species, ultimately resulting in a set of ordinary differential equations. In the present example, the concentrations of observed gas phase products are the "response variables" which are used to achieve a fit and measure the goodness of the fit (there are also intermediates in the model that do not appear among the response variables). In this work, we have used Athena Visual Studio (a commercial program) for the simulation. Other numerical simulation codes do exist and some are listed in Section S.VIII of the Supporting Information. The experimental data was previously published [1], and was provided by Mullins.

2.1. Reaction model and initial parameters

The model formulation and the initial parameters (Steps 1 and 2) were developed utilizing published studies and chemical knowledge. That process is described in a separate work which focuses on the chemistry of the mechanism [53]. The reaction model and the values of the initial parameters used are provided in Section S.·I. of the Supporting information, along with the corresponding differential equations. With an established reaction mechanism, we move forward to transformation of the experimental data. Section 2.2 concerns a procedure for transformation of mass spectrometry intensities to concentrations, followed by Section 2.3 which applies to the more general process of what was done once concentrations were obtained.

2.2. Experimental data transformation: scaling mass spectrometry intensities

Transforming the experimental data (Step 3) consists of several SubSteps, which will be numbered "3-N″ where N is the number of the substep. The first SubSteps are aimed at converting the experimental data to signals that are scaled to concentration. Mass spectrometry data is the type of data most commonly used in TPR analysis in the field of surface science and catalysis, and is the source of the data used in this study. The data transformations that convert the mass spectrometry signals to concentrations are described in this section.

In the case of mass spectrometry data, we have adapted a method that has been published by Madix and Ko [54], which corrects for the sensitivity of the mass spectrometer to different mass ranges etc. When each product cannot be calibrated separately for the mass spectrometer used, we believe that at minimum a modified version of the method of Madix and Ko should be used (the author is not aware of other methods of comparable accuracy and precision in the absence of direct calibration). The intensity correction procedure used for CRN-TPR is the same as it would be for simple reaction network TPR. However, fitting of CRN-TPR is more sensitive to the calculated ratios of the products, since this affects the fitted pathway selectivities and mass balance, and consequently it is more important to perform such intensity corrections (which are not always done with simple reaction networks). The process can be thought of as consisting of 4 sub-steps after the signal's background correction, which is referred to as Step 3–0 here. Background correction can be a bit of an art and requires interpretation of the data. In this work, the approach that was taken was that all experimental signals that we did not have evidence for neglecting were retained to see if the simulation and fitting were capable of producing those signals. There are other legitimate approaches to background corrections, but a discussion of the various approaches for interpreting signals as background vs. relevant is beyond the scope of this work (which focuses on steps later than background correction). For the purposes of this work, we only note that background correction is important. Step 3–0) Background corrections must be performed on the raw signals for each mass, prior to applying the intensity corrections in the following steps, otherwise serious concentration inaccuracies can be introduced in the final ratios. Step 3–1) a mass dependent gain correction (G_M) and mass dependent transmission probability correction (T_M) are applied to each mass to correct for mass dependent sensitivity – this produces a spectrum where the intensity is proportional to the concentration of ions for each mass fragment. Step 3–2) the spectrum is normalized to have the intensities sum up to 1 (or 100). Step 3–3) divide the normalized intensity of a particular mass fragment by the total ionization efficiency (I_x) of the parent molecule to obtain a scaled concentration (proportional to partial pressure) of the parent molecule. If multiple parent molecules contribute to particular mass signal, then separate terms must be added for each parent molecule's contribution. After the preceding 3 sub-steps, the scaled concentrations of the parent molecules (i.e., reactant and product gases) can be directly compared to each other as they are in units that are directly proportional to concentration. A fourth but optional step, Step 3–4), is to use calibration of one of the molecules to scale the signals of all molecules to torr or some other non-arbitrary unit. Step 3–3 can be performed either using hand-picked masses (as done by Madix and Ko [54]) or by using a set of linear equations to describe each mass number and its relationship to each parent molecule that can be solved with matrix methods (or other methods). The matrix methods are prone to giving unreasonable results, such as negative concentrations, if appropriate background corrections are not performed in step 3–0 and when there are deviations in the real fragment patterns from the reference fragment patterns.

For most mass spectrometers, the mass dependent correction terms in Step 3–1 will not exactly follow the functional form used by Madix and Ko [54], since each mass spectrometer has different tuning. Consequently, the best procedure is to utilize known concentrations of gases with several molecular weights and cracking patterns (such as mass spectrometry calibration gas mixtures) to find an approximate functional form for correcting the mass dependence of signals obtained with a particular mass spectrometer. When calibrations of the gases expected are not possible, using the cracking fraction of several relatively heavy hydrocarbons such as hexane can enable extraction of a functional form that can describe the tuning of a particular mass spectrometer, which can then be used to in conjunction with reference mass fragmentation patterns to obtain the mass dependent correction function. Failure to make corrections for an individual mass spectrometers' tuning can result in inaccuracies in the concentration ratios for species with substantially different molecular masses (e.g. a factor of 6 scaling difference between mass 60 versus mass 15). After calibration, care must be taken to be aware of sources of variability and inaccuracy (e.g., the tuning and response of a mass spectrometer can drift during timescales on the order of months).

We note that processing or reprocessing the data with the above procedure is burdensome for CRNs when a change must be made - for example, if a signal previously attributed to a molecule such as ethyl acetate becomes reinterpreted as being due to another molecule such as acetone, or if a revision is made to the calibration curve, or if the background of a mass contribution is re-interpreted, etc. It would be desirable to have a versatile and user-friendly computer program which

can easily re-apply the procedure in light of new data, new interpretations, or new calibrations, and we are working on developing such a program.

2.3. Experimental data transformation (and objective function): integral production

Prior to discussing CRN-TPR data transformation, it is instructive to consider what happens during fitting of more simple reaction networks. When fitting a simple first-order temperature programmed desorption from a surface (TPD_S) with a two-parameter fit (pre-exponential and activation energy), an adequate fit can be obtained with a good initial guess of the pre-exponential and activation energy and fitting the rate of desorption versus time. However, if the initial guesses are *not* near the final values (e.g., within a factor of 10 for the pre-exponential and a factor of 10% for the activation energy) then gradient based parameter optimization routines typically get stuck in undesirable local minima (i.e., they do not find a good fit when fitting the rate of desorption versus time). Gradient fitting faces additional challenges with real experimental data, due to the roughness in the objective function surface produced by noise. A difference in the fitting of CRN-TPR (relative to simpler reaction networks) is that these challenges are further exacerbated by discontinuities that can arise in the objective function surface due to the possibility of changes in the operative mechanism when the kinetic parameters are varied (i.e., the dominant pathway can change). For the above reasons, a decision was made to convert the rate of production into integrated production, which also provides several advantages during fitting. A) Convergence to a good solution without getting stuck in a local minima is facilitated by this procedure since the function produced is monotonic as a function of distance from the optimal value (in each direction), leading to a more well shaped landscape for the residuals in the global parameter space – this is shown in Fig. 1 for the example of a first order desorption process. Fig. 1a shows that when varying the simulation activation energy, the squared sum of residuals (SSR) of the response (i.e., for the simulation output versus data for fitting) becomes relatively flat at a short distance away from the "true value", while Fig. 1b shows that the integrated response curve has a dependable valley shape which continues infinitely in both directions as a function of distance from the "true value". During test fittings, it was also found that simulation and fitting of ideal data (data which was simulated using the rate equation employed) converged to a global optimum more easily after conversion to integrated production. Perhaps unsurprisingly, for nonideal data, it was found that sequential parameter optimization consisting of optimizing the activation energy first with the pre-exponential fixed, followed by allowing the pre-exponential to vary, was the best strategy for achieving a good and meaningful fit. B) As other authors have noted, using the integrated area reduces the effects of experimental noise (see Fig. 2) [33,55]. Consider that if half of the noise involves a positive error while half the noise involves a negative error, then these errors should cancel in the integrated area, and this effect contributes to the smoothness of the integrated area curve shown in Fig. 2. In addition to this cancellation in the sum of the noise, the effects of small peaks or outliers created by noise will affect the residual less strongly in the integral production curve. Observe that in Fig. 2 there are discontinuities and peaks at the beginning and end of the experiment, but that these are small in magnitude and less apparent in the integrated production curve. C) The time resolution required in the data to achieve a good fit while capturing the necessary behavior is significantly decreased, which reduces the number of points needed during parameter optimization and enables more rapid fitting computations. D) Plotting the integral production curve also enables facile estimation of the stoichiometric ratios of various product peaks even when multiple peaks are present.

Some of the advantages of using the integrated area on real experimental data are illustrated in Fig. 2, which shows data related to production of formaldehyde gas with a temperature programmed reaction of methanol over $CeO_2(111)$ [53]. Fig. 2A shows the rate of production for formaldehyde in arbitrary units with smoothing and without smoothing. In Fig. 2B, the integrated production curves are nearly identical (i.e., the integrated production curve is inherently smooth). There are several features in Fig. 2 worth noting: 1) the unsmoothed data includes significant noise, which would result in undesirable local minima during parameter optimization if the rate of production is used instead of the integrated rate of production 2) there are discontinuities and peaks near the beginning and the end of experiment in the rate of production data (including a sharp negative peak near the beginning), which could result in significant residuals during fitting. However, these troublesome features in Fig. 2A are not apparent in Fig. 2B, because conversion to the integrated production diminishes the effects of such features, leading to fewer problems during parameter estimation. 3) Peaks in the rate of production (Fig. 2A) show up as steeper slopes in the integral production (Fig. 2B), such that the "peaks" remain as distinct features for parameter estimation when using the integrated production curve.

We note that if smaller peaks are of mechanistic importance, then they should be resolved (the signals separated) and each associated with a separate response variable. For example, if chemical A is produced by two different pathways at different temperatures, then these two peaks should be treated as separate responses such that they have separate sums of squared residuals. A concrete example of resolving such peaks is shown in Fig. 3, using the methanol gas phase response from the same experiments as Fig. 2 and applying the simple

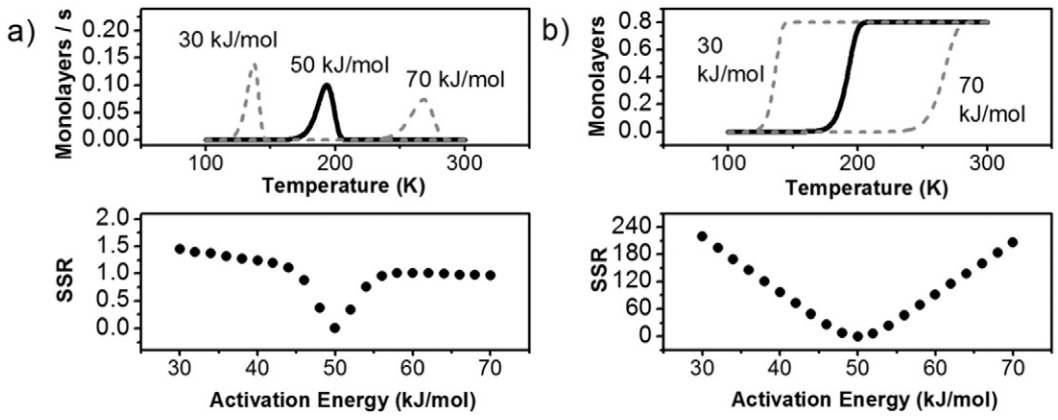

Fig. 1. Upper plots show the rate of production curves (upper left) and the integrated production curves (upper right) for temperature programmed desorption with 50 kJ/mol versus 30 and 70 kJ/mol. Lower plots show the landscapes for the corresponding sums of square residuals (SSR) as the activation energy is varied, for the case where the true activation energy is 50 kJ/mol. As described in the text, the integrated production curve has an SSR functional form that has advantages when estimating kinetic parameters as part of a complex reaction network. In these simulations, an Arrhenius form was assumed with $10^{13} \cdot s^{-1}$ for the pre-exponential, 2 K/s for the heating rate, and an initial relative coverage of $\theta_0 = 0.8$.

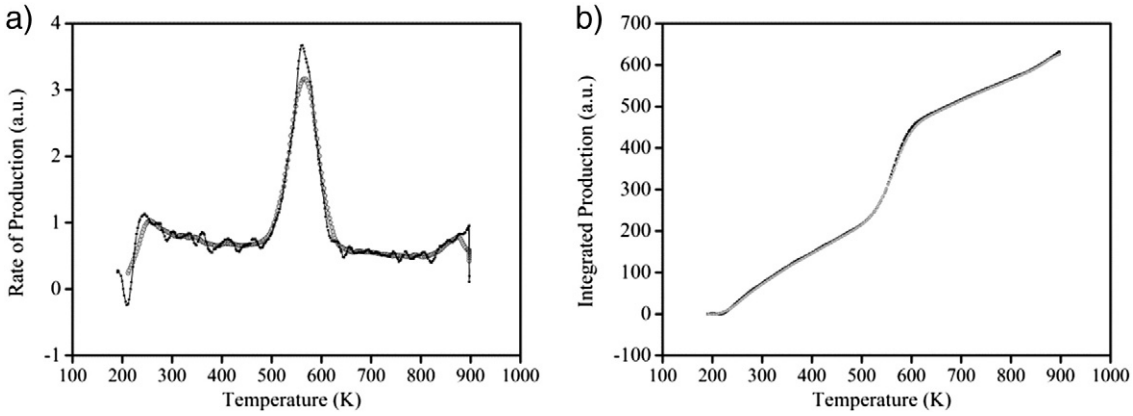

Fig. 2. Data for the rate of production (2A) of the experimentally observed formaldehyde gas, alongside the same data converted to integrated production (2B), in arbitrary units. The black points correspond to data which has been background corrected but not smoothed, while the gray points correspond to the case where the data was smoothed prior to integrating. The two curves are nearly identical in 2B, illustrating that conversion to integrated production helps to mitigate the effects of noise and discontinuities during fitting even without smoothing.

method of interval splitting (though other methods exist). Note that the small peak near 550 K is clearly visible in the integrated production both before and after resolving, but that when analyzing residuals the smaller peak contribution can be swamped by the larger peak's residuals if such peak resolving is not performed. During simulation and fitting, such separations should be performed if a minor contribution is of importance, and separate response variables and state equations are then required to describe the resolved peaks (resolving such features also facilitates more meaningful weighting during parameter estimation, See Section 2.5).

There were several SubSteps in this part of the experimental data transformation: 3–5) background subtraction (important), 3–6) smoothing the data (optional), 3–7) threshold filtering (optional), 3–8) interpolation (optional). As noted above and elsewhere [55], subtraction of background signal, SubStep 3–5, is very important if an integral curve method will be used, as even a small spurious background signal will result in error in the production or depletion of the monitored species that becomes compounded across the time of experiment. The procedure for baseline subtraction for CRN-TPR is the same as for the case of simple reaction networks. However, baseline subtraction has increased importance for CRN-TPR because when there are branched reaction pathways the expected selectivity/stoichiometry of competing pathways may be distorted when no baseline subtraction is performed (and distorted stoichiometry/selectivity can make the fitting significantly more challenging). In principle, the least-work option to deal with a background signal would be to include artificial processes to reproduce the background signal (for example, a constant background could be described by a process with a 0 order kinetic rate equation to produce that species, where the added process requires no reactant). However, adding-in processes to reproduce background signal also adds another adjustable parameter, and can result in unintended consequences during parameter estimation. Due to the large number of parameters already present in CRNs, and the advantages of human judgment in baseline subtraction, we recommend that background signals instead be subtracted beforehand with visual inspection.

We found that interpolation to a smaller number of points, Step 3–8, also known as "thinning", could be done with little loss of information in the residuals of the integrated production curves (see Fig. 4). This reduction in the number of datapoints for the response variable was highly desirable as the time for each iteration during simulation and fitting for parameter optimization was drastically reduced by having fewer points to fit. Such thinning would not be as effective when the rate of production is used rather than the integral of production. Our procedure applies all filters and smoothing prior to extracting this smaller number of points for kinetic analysis (as recommended elsewhere [26] for analysis of temperature programmed reaction data). In our case, the data was scaled to the monolayers unit (ML) between SubStep 3–7 and SubStep 3–8, using the assumption that the sum of all carbon containing gas phase species detected by the end of experiment was equal to 1 monolayer (i.e., stoichiometric to the number carbon containing molecules on the surface at the start of experiment).

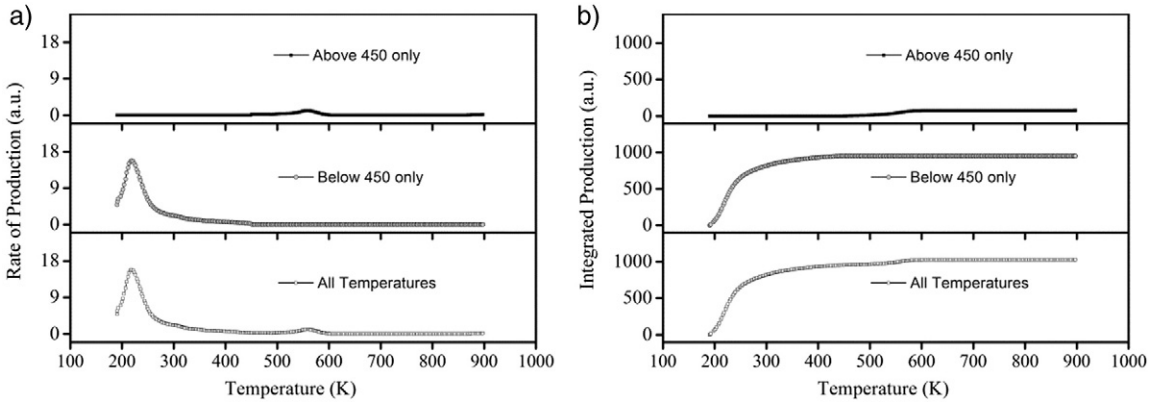

Fig. 3. Rate of production (3A) and integrated production (3B) of the experimentally observed methanol gas, in arbitrary units. The 3 vertical layers show data from different intervals to illustrate peak resolution by interval separation. From bottom to top the layers show: production from the full temperature range, production below 450 K only, and production above 450 K only. Using this interval method, or other methods for resolving signals prior to simulation and fitting, can be very useful when smaller features (such as the peak near 550 K) are mechanistically important.

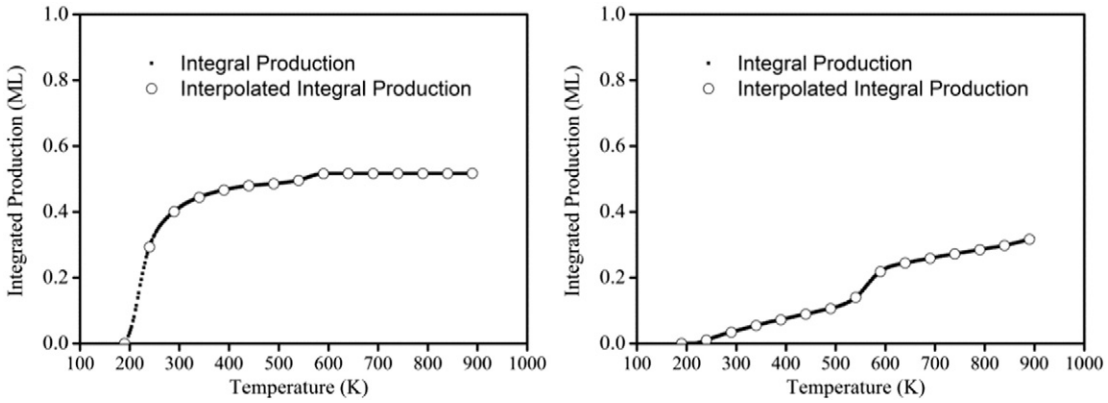

Fig. 4. Integral production for the experimentally observed methanol gas (left) and formaldehyde gas (right) in monolayer units. Data is shown for each collected experimental data point after SubStep 3–7 (dark squares), as well as the interpolated integral production after SubStep 3–8 with 50 K increments (open circles).

When attempting to assess the correctness of a chemical model with the aid of kinetic simulation of a temperature programmed reaction, there are significant benefits in using multiple heating rates and/or initial coverages; [21,22,33,34,46,48,49,56–59] or using temperature programs more complex than a linear temperature ramp [22,57,58, 60–64].

2.4. Stiffness mediation during simulation

When using ordinary differential equations to simulate temperature programmed reactions, stiff equations are encountered. For simple reaction networks, implicit ODE solvers or dynamic stepping methods can be *necessary and sufficient* to overcome the stiffness [26]. For CRN-TPR, implicit ODE solvers and dynamic stepping methods are *not sufficient*, as described below.

One of the types of numerical instability errors encountered can be demonstrated by a simple first order temperature programmed desorption from a surface (TPD_S) simulation using Euler's method and inputs of a Pre-exponential of $10^{13}\cdot s^{-1}$, a heating rate of 2 K/s, an activation energy of 50 kJ/mol, an initial relative coverage of $\theta = 0.8$, a starting temperature of 100 K, and a time step size of 0.1 s, as shown in Fig. 5. Two forms of numerical errors occur due to the exponential growth of the rate constant with temperature. The first type of numerical error occurs near 217 K when the coverage becomes negative but remains close to 0 (not visible in Fig. 5). This occurs once the rate of depletion is sufficiently larger than the remaining concentration for a given integration stepsize. From that point on, the coverage bounces between positive and negative with each alternating simulated point. At this stage, there are numerical errors, but the solution is still stable. The second and more serious type of error occurs at higher temperatures (before 240 K in Fig. 5), when the rate constant becomes sufficiently large that the rate of reaction becomes too large to be simulated with a given stepsize, resulting in a change in coverage that increases the magnitude of the coverage (which itself also increases the rate in an autocatalytic manner). At this point, the Euler's method solution to the differential equation has become *unstable*, ultimately leading to a rate and coverage that bounce between positive and negative infinity.

The type of error displayed in Fig. 5 is caused by the stiffness of the rate equation and has been described by Caballero and Conesa [26] who provide two possible solutions. The first is setting the rate of change to be 0 below certain threshold concentrations as well as after achieving a negative value, which can prevent the instability for simple reaction networks such as the first order desorption process shown in Fig. 5. However, as noted by Caballero and Conesa, that approach only works in some cases and can introduce significant numerical errors. Essentially, this first method method prevents numerical errors by zeroing the depletion prior to the temperature where the resulting errors become too large in magnitude. This method is only safe if a reaction network contains solely depletion of species. In a CRN, there is a risk that an intermediate on the surface will be *produced* "suddenly" under conditions where a rate constant for depletion of that intermediate has already become very large. Thus, the first method cannot be used for a CRN. The second method provided by Caballero and Conesa [26] is to increase the time resolution of the simulation (i.e., decrease the step-size) – either over the whole simulation or in the area of stiffness. As pointed out by Caballero and Conesa [26], Matlab ODE23 has dynamic stepping time resolution built-in to its algorithm and thus includes the second method on the fly. However, dynamic stepping is not a viable route

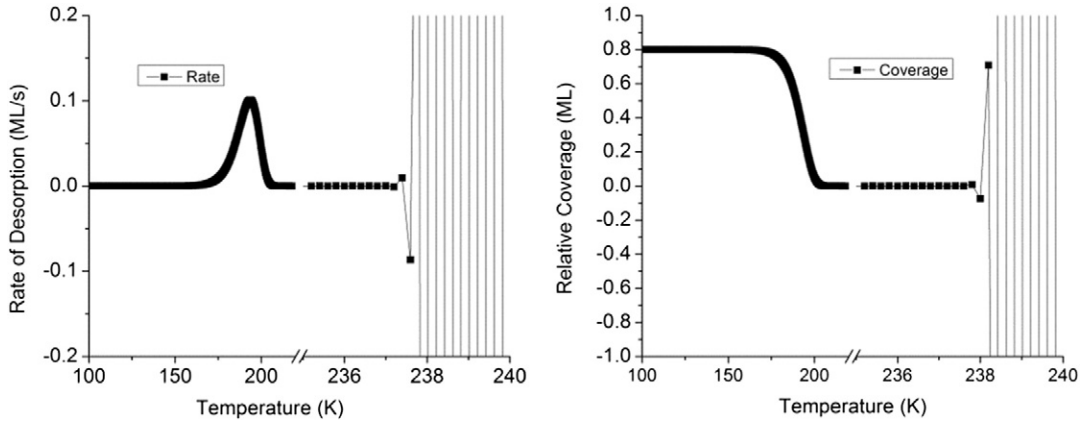

Fig. 5. The rate and relative coverage of a sample TPD_S simulation using Euler's method is shown (see text for details). At temperatures not much higher than the desorption peak maximum temperature, numerical errors occur due to the stiffness of the rate equation.

for temperature programmed reaction experiments with CRNs: the rate constants which have low activation energies will become stiff and require simulation with impractically high levels of time resolution or numerical errors prior to reaching conditions relevant to processes of interest at higher temperatures.

Caballero and Conesa [26] pointed out that for the situation plotted in Fig. 5 (such as for first order desorption processes) the instability can be prevented by using an implicit ordinary differential equation solver, such as Matlab ode23s. In contrast, the CRN-TPR simulations performed in this study *already* use an implicit ODE solver and *still* encountered instability errors of the same class displayed in Fig. 5 (Athena's ODE solver is DDAPLUS, which is based on Gear's method, which is an implicit ODE solver). We note that for sufficiently simple reaction networks, such as for the first order desorption process shown in Fig. 5, Athena does successfully simulate the TPD peak without any numerical instability. The fact that even the implicit ODE solver used by Athena encountered numerical instability from the coupled equations present in CRN-TPR is a different and further challenge relative to simulation and fitting of more simple reaction network TPR. To reiterate: for simple reaction network TPR, either implicit ODE solvers or dynamic stepping methods are sufficient, but neither method (nor both together) is sufficient for CRN-TPR. After consideration of the source of numerical instability, a regularization method was used for stiffness mediation of high rates (described in Section S.·V of the Supporting information) to prevent the instability encountered otherwise. For other experimental conditions (such as in a flow reactor with a constant source of reactants), or if greater accuracy is required, alternative methods for separation of fast processes may need to be used as part of the stiffness mediation – some methods and general ideas have been discussed elsewhere [65–78].

2.5. Weighting of data points

Weighting of data points is important to allow for minor pathways and minor products to have an appropriate level of influence on the calculated goodness of fit during fitting. As noted in the discussion of Fig. 3, this can benefit from separation of minor but important pathways into separate response variables prior to weighting. Having done that, we proceed to weighting. Separating minor pathways can play a role of increased importance in CRN-TPR since the optimization process is already difficult (due to the larger number of parameters and potentially larger number of response functions), and when branching is present the minor pathways are less easily captured correctly unless appropriate weighting is applied.

In our final objective function, two commutative weighting factors were used for each data point in line with practices described by NIST and others [13,31,79]. 1) a $1/y_i$ weighting factor was chosen to compensate for the magnitude of minor products as well as low value data points, where y_i, is the experimental value of the response variable at a given data point (i.e., at a given time/temperature). Note that this weighting factor also enables small features as described in Fig. 3 to be fitted properly provided that they are properly resolved prior to fitting. 2) a weighting factor to compensate for variance and other errors was used, $1/(REE)_i$^2, where $(REE)_i$ is the relative estimated error of a given experimental data point (here taken as the greater of 10% of the value or 0.01 monolayers). The two weighting factors were multiplied for each data point to create combined weighting factors (e.g., for a value of 0.2 monolayers the combined weighting factor for this work was $(1/0.2) * 1 / ([MAX(0.01,0.1 * 0.2) / 0.2] * 100)^2 = 0.05$). Values where the response was 0.0 were given a combined weighting factor of 0.0.

In our analysis, the data were evenly spaced prior to parameter optimization. The use of the objective function based on a weighted SSR (WSSR) from the integrated production worked well partially because the residuals are proxies for the differences in areas under the simulated and measured curves. If the data are not evenly spaced during fitting, then an additional commutative weighting factor can account for the uneven spacing, with an additional weighting factor based on $x_i - x_{i-1}$ (where i is the index of the data-point and x_i is the abscissa value at that point).

2.6. Objective function and parameter optimization

During parameter optimization of CRN-TPR, we found the key to a successful parameter optimization was to have an appropriate objective function, with appropriate weighting of each data point. Ideally, a well chosen objective function will enable two things 1) sensitive discrimination between the goodness of fit for parameter choices and 2) the use of methods for finding a better fit, such as gradient optimization. In the lower panels of Fig. 1, we see the functional forms that arise for a first order desorption process while varying a single parameter and taking the objective function to be either the SSR of the rate of production or the SSR of the integrated production. The optimal value for the activation energy in Fig. 1 is the location of the minimum in the objective function in either lower panel (both lower panels have the same minimum, and thus the same optimal value). As seen in the lower panels of Fig. 1, the functional form that arises from the SSR based on the rate of production qualitatively resembles a dirac delta function, while the functional form that arises from the SSR based on the integrated production qualitatively resembles a parabola. Extending these concepts into the higher dimensional space created during parameter optimization of a CRN, we would expect that a) in the case of SSR based on the rates of production, the higher dimensional space will be relatively flat, punctuated by steep drops when particular parameters are near their local optimums, and that b) in the case of SSR based on the integrated productions, the higher dimensional place should have gradual curves when individual parameters are changed, creating slopes/valleys to enable detection of the correct direction towards the local optimum. This will be shown to be true, and is the crucial point of the present work: that for simulation and fitting of the chemical kinetics of CRN-TPR, use of the SSR for the rates of production will not provide a desirable objective function for optimization (due to consisting of a flat multi-dimensional surface punctuated by drops), while use of an objective function based on the SSR for the integrated productions will provide a suitable objective function for optimization (due to consisting of gradual slopes towards local optima on the multi-dimensional surface of parameter space). Thus, use of an objective function based on the integrated production can enable sequential optimization of parameters, and the final objective function used here was based on the WSSR of the integrated productions of the gas phase products.

For the example system described here – temperature programmed reaction of methanol over $CeO_2(111)$ – the species, the kinetic rate equations, and the parameter values for the initial model are provided in Sections S·I and S·II of the Supporting information (>40 parameters). Fig. 6 shows both the integrated production curves and the rate of production curves for the six response variables (simulation versus experiment [1]), when using initial values for the parameters based on the literature which we call “Model 1”. the only chemistry which is observed is desorption of methanol (CH_3OH). From here, there are several ways to optimize the kinetic parameters. A discussion of parameter optimization methods is provided in Section S.·VIII of the Supporting information. Essentially, the parameters must be varied, but with >20 parameters the parameter space is too large to explore completely. Instead, the parameters must be varied sequentially, and some metric for progress towards a better fit (the objective function) must be used along with gradient optimization. It should be emphasized that with such a vast parameter space to explore, it can be hard to find *any* reasonable fit, even if the initial model has parameter values that are close to the optimal fit. This will be shown to be the case for the present system, and is partially because the operative mechanism (pathways accessed) can change within the simulation of the CRN-TPR as the parameters are changed: this means that simulation and fitting routine is essentially exploring a set of objective function

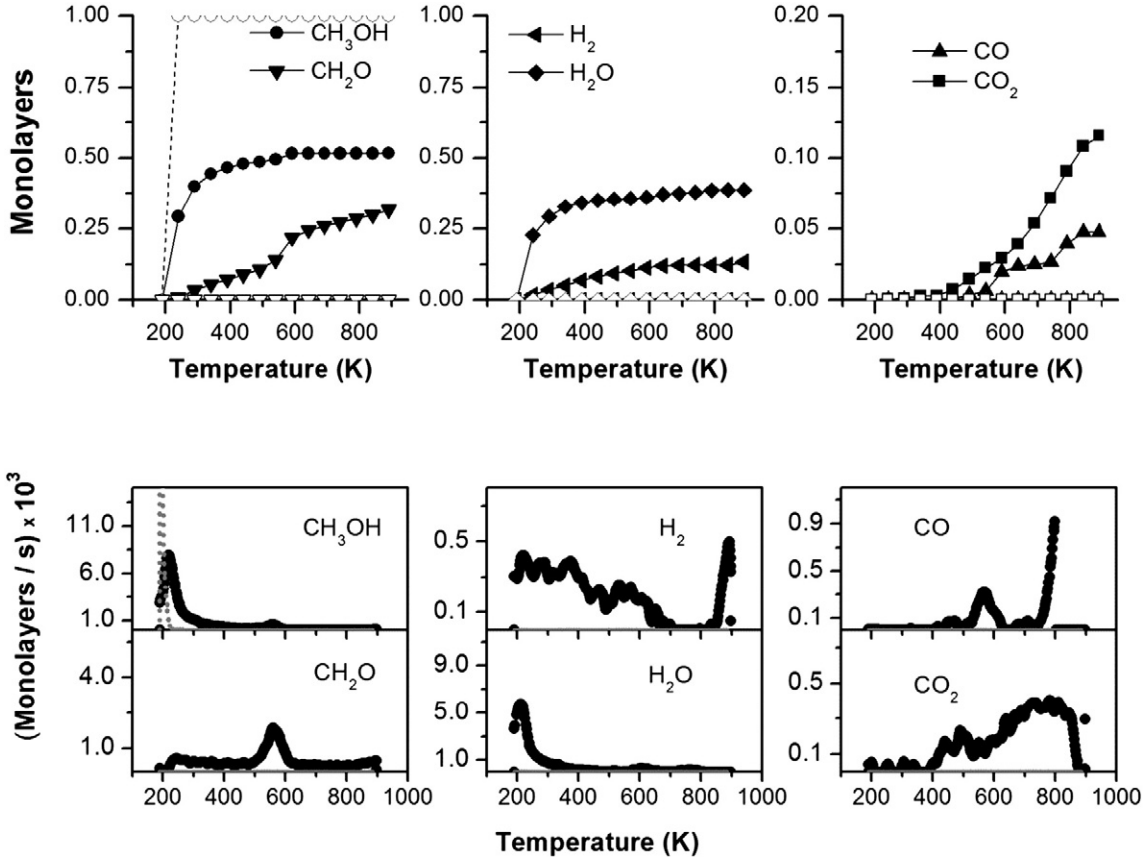

Fig. 6. Integrated production (upper graphs) and rate of production (lower graphs) for observed gases. Filled symbols: experiment. Open symbols and dotted lines: Simulations using Model 1. Using Model 1, almost the only chemistry observed is desorption of CH_3OH.

surfaces rather than a single objective function surface (i.e., if changing parameters changes the route the reaction network takes, then the simulation has jumped to a different objective function surface). The fact that there may be multiple objective function surfaces to explore – and thus multiple solutions [19] – is one reason that it is important to check multiple initial parameter values [13,21,33,55], as was done in the present study. By following the procedure in this study, improved fits were achieved, and one is shown in Fig. 8. Clearly, Fig. 8 is an improved fit relative to Fig. 6. This was achieved using objective function described above and by varying the parameters over ~60 iterations.

The objective function values during ~60 iterations of model adjustments are shown in Fig. 7. Each bar in Fig. 7 represents the final objective function of a different model (i.e., after one iteration in the optimization process), thus each bar reflects different kinetic parameters and/or changes in the reaction mechanism. The bars in Fig. 7A correspond to the objective function which was successful in providing improved fits in this work (based on integrated production), while the bars in Fig. 7B correspond to the objective function which was not found to be useful in this work (based on the rates of production) are shown. The seven red bars correspond to "Numbered models" for which the kinetic parameters are provided in Section S.·I of the Supporting information (these are termed "Model 1" through "Model 7"), while the blue bars correspond to additional models for which qualitative information was tabulated in Section S.·I of the Supporting information. The simulation output for the right-most red bar, Model 7, is shown in Fig. 8. The model 7 output in Fig. 8 can be considered a more reasonable fit to the data relative to the Model 1 output in Fig. 6.

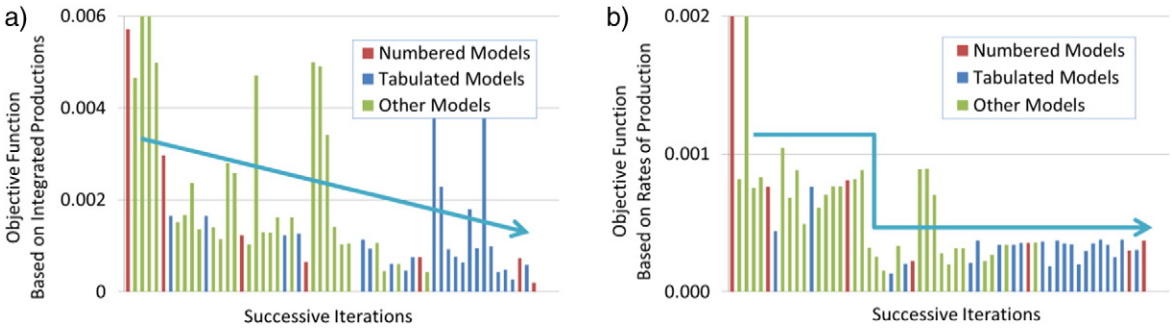

Fig. 7. A) and B) show the behavior of the objective function based on the integrated productions and rates of production, respectively, for ~60 models ("successive iterations") during optimization. Each bar represents an additional model (additional iteration) in the optimization process. The objective function surface based on the integrated productions is more responsive to parameter changes, so shows a trend of a gradual decrease as well as jumps. The objective function surface based on the rates of production is better described as a "flat" surface punctuated by steep drops, and provides less guidance during optimization.

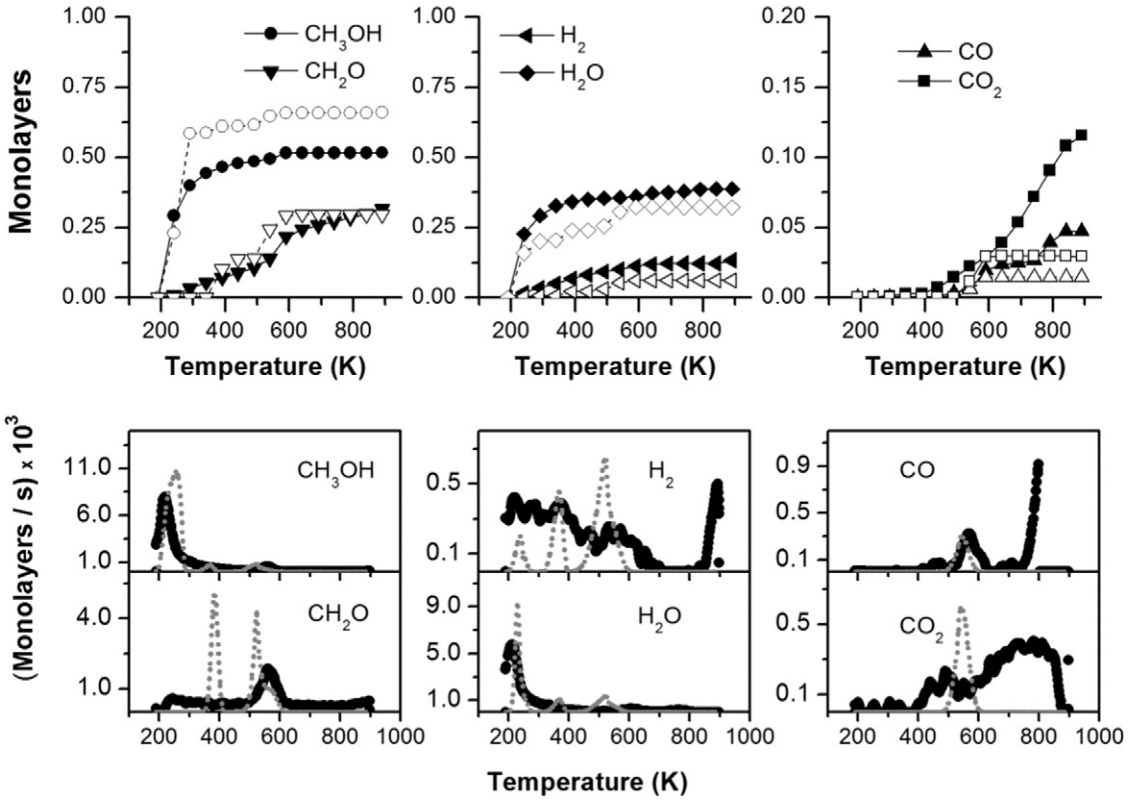

Fig. 8. Integrated production (upper graphs) and rate of production (lower graphs) for observed gases. Filled symbols: experiment. Open symbols and dotted lines: Simulations using Model 7. Model 7 achieves a more reasonable fit than Model 1 (compare to Fig. 6).

Model 7 includes some coverage dependent activation energies and the H_2O production occurs by a mechanism where both hydrogens originated from the alcohol hydrogen in methanol with no low temperature C—H bond breaking pathway [53]. As discussed in Section S.·VI of the Supporting information, the role of simulation and fitting is to show that a particular model is plausible, not that it is correct [58,59]. By starting with an initial reaction network and kinetic parameters, it was possible to get an improved fit relative to experiment (sufficient to show that the proposed reaction network was plausible). A perfect fit was not the goal – only to show the plausibility of various mechanistic choices. As shown in Section S. IX of the Supporting information, all 7 of the "Numbered models" only required small adjustments in activation energies from the original parameters obtained based on current knowledge (typically changes of <20% from the initial guesses and within 20 kJ/mol – which is within the error of density functional theory and the current knowledge). Thus, through guided exploration of parameter space, while staying within realistic base activation energy values, we have been able to show that the complex reaction network consisting of the reactions in Table S.1 of the Supporting information is a *plausible* explanation of the data. Without the methods described in this work, we would have been unable to find the improved fits to show this plausibility.

Each of the seven numbered models has different mechanistic implications. Once these various 'reasonable' fits were found, the mechanistic implications could be considered and compared to the body of knowledge available. The mechanistic implications of the seven numbered models are beyond the scope of this work, and are discussed in a separate study [53].

A few comments should be made about the bars in Fig. 7A and B, where the optimum sought is a minimum. The first point is that the crucial issue described at the beginning of this section is visible in Fig. 7: Fig. 7A shows a gradual approach to an optimum for the objective function, while Fig. 7B shows a more flat surface. The second point is that the "jaggedness" within the downward trend of Fig. 7A is not a demonstration of weakness of the recommended objective function – rather, it is a demonstration of strength that the recommended objective function can identify when a parameter (or parameters) are moving in the wrong direction, unlike the objective function in Fig. 7B which tends to remain more flat *even* when a parameter is being adjusted in the "wrong" direction. The source of these differences can be seen in Fig. 1. Essentially, when a simulated peak does not overlap with the experimental data, the residuals from the rate of production shows nearly no change in residuals when a relevant kinetic parameter is varied. In contrast, even when a simulated peak does not overlap with the experimental data, the integrated production shows a gradual change in the residuals when a parameter is varied (as shown in Fig. 1, lower panel). This enables finding an improved fit where the simulated and experimental peaks overlap or are closer together. As shown by Figs. 1 and 6, this concept holds for TPR of both simple and complex mechanisms, and with either one or many adjustable parameters.

It is possible to show the benefit of using the integrated production by plotting a color-map of a cross section of the parameter space. Fig. 9 shows that a 2D exploration of the parameter space in the vicinity of the optimal solution for model 6 confirms that the objective function based on WSSR of the integrated production is a well behaved objective function while using the SSR of the rate of production is not. It can be seen that the SSR based on the rate of production has multiple maxima and minima, with surface contours that would not enable gradient optimization to find the optimum unless the initial guess was very close. In contrast, the objective function based on the WSSR of the integrated rate of production enables gradient optimization to find the optimum from nearly anywhere in the parameter space explored. This color map only shows the contours for varying *two* parameters: in this study, the number of parameters varied was on the order of 10 (so >100 such cross sections could be plotted) and the greater the number of parameters varied, the more important a well-behaved objective function surface becomes. More details about the models, including the rate equations and parameters utilized, are available in the

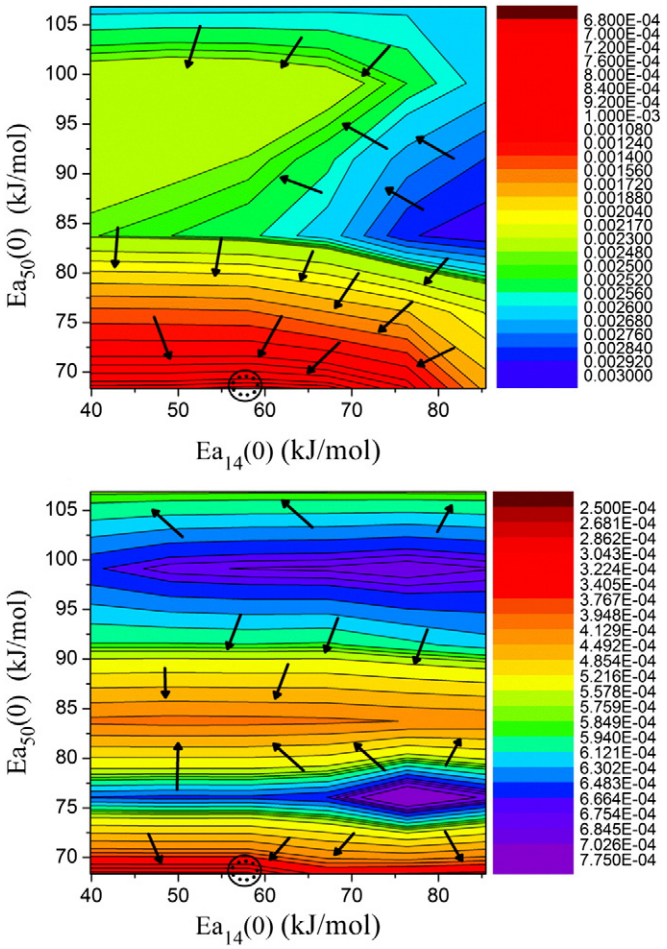

Fig. 9. Surface plot corresponding to the WSSR of the integrated production (upper plot) and surface plot corresponding to the SSR of the rate of production (lower plot). These surface plots represent partial exploration of the parameter space near the optimized values for Ea_{50} and Ea_{14} which correspond to the methanol desorption and water desorption. Red values are optima. The upper plot is a more well behaved objective function for gradient optimization. The circle of dots represents the optimized value, and would not be found by gradient optimization using the lower plot unless the initial guess was already very close to the optimum.

Supporting information. The Supporting information also includes graphs of integrated production curves and rate of production curves for the seven models with red bars, to show the gradual progress that occurred during the optimization process. As always, researchers must consider information that may be outside of the objective function: Though it is beyond the scope of this work, we note that Model 6 (the second last red bar) was considered to be in better agreement with experiment than Model 7 (the last red bar), based on the nature of the intermediates present from 400 to 500 K in the simulations versus experiments.

3. Conclusions

For a CRN-TPR that has many kinetic parameters it is difficult to find any reasonable fit during simulation and fitting – partially due to the vast parameter space. However, such fitting is necessary to ascertain the plausibility of a reaction mechanism and kinetic model being considered. This difficulty remains even when the initial guesses of parameters are close to those of a reasonable fit. Fortunately, when trying to show the plausibility of a reaction mechanism and kinetic model in CRN-TPR, a perfect fit is not required: merely the production of the correct species in the correct temperature range. In this work, simulation and fitting of a CRN-TPR was performed to show the plausibility of a kinetic model being investigated, with the intent of establishing a method and comparing two possible types of objective functions. A perfect fit was not obtained, but an improved fit was obtained (the initial literature parameters resulted in only desorption of the starting reactant, while the final fits showed the correct products in the correct temperature ranges). It was found that the key to obtaining improved fits was having an appropriate objective function. The conclusions and findings from this work can be summarized as follows:

1. The objective function that was found to work well in this work was a weighted sum of squared residuals for the integrated productions of the various species (responses). This is the most crucial point of the current work: that the shape of the objective function surface created by using the integrated production will have gradual approaches to local (and global) optima. In contrast, an objective function surface based on the SSR of the rate of production will be relatively flat, punctuated by steep drops, which is undesirable for parameter optimization. This phenomenon is demonstrated to occur for both simple mechanisms (lower panels of Fig. 1) and complex mechanisms (Figs. 7 and 9).
2. The use of integrated production has additional advantages: it suppresses effects from experimental noise, requires much fewer points to describe the response behavior (which allows thinning and decreases the computational cost for simulation and fitting), and can be simulated numerically with small errors.
3. Implicit integration methods are not sufficient to prevent numerical errors from coupled equations in CRN-TPR, and algorithms which rely heavily on changing the time step size dynamically are also insufficient. One strategy is piecewise mediation of the stiffness of the expressions of the rate constants, with re-evaluation of the rate expressions for each species at each time-step.

The following points also apply for simple reaction network TPR and are not new concepts, but have increased importance for CRN-TPR relative to simple reaction networks:

4. Appropriately weighting and separating/resolving small peaks will add to the effectiveness of correctly fitting minor products and minor pathways.
5. During parameter estimation/objective function optimization, when the rate constants are Arrhenius or Arrhenius-like, it is beneficial to allow non-integer values for the power of the pre-exponential and vary the power of the pre-exponential (rather than varying the pre-exponential directly).
6. When direct calibration of individual mass spectrometry signals is not feasible, other methods should be used. One method for converting mass spectrometry data to a form that is proportional to concentration is to use an adapted version of the method of Madix and Ko (we believe this is the minimum level of accuracy required for fitting).

Note added in review

One of the reviewers pointed out that it is very important to account for experimental factors, such as the sample mount and heater system. Important factors include how background partial pressures vary with time, the accuracy of the thermocouple temperature (i.e., location of the thermocouple), design of the sample holder, as well as the proximity and 'line of sight' with the mass spectrometer. There are also 'tricks' such as degassing the sample and sample holder prior to adsorbate exposure, or (as pointed out by the reviewer) the trick of sputtering off a portion of the adsorbates – which is different from dosing a lower coverage, and can help to differentiate spurious signals. The author of this work agrees with the reviewer that knowledge of such experimental practices is very important. In fact, the author believes

that an entire publication could be written on the subject of mitigating and subtracting backgrounds from TPD experiments, and the author hopes that a member (or members) of the community will write such a publication.

Acknowledgements

This work was supported by the U.S. Department of Energy, Office of Science, Basic Energy Sciences, Chemical Sciences, Geosciences, and Biosciences Division (ERKCC96). A. Savara thanks David R. Mullins for providing experimentally obtained TPR data and for useful conversations, and Michael Caracotsios for instructions on the basic use of Athena Visual Studio modeling and estimation software.

Appendix A. Supplementary data

Supplementary data to this article can be found online at http://dx.doi.org/10.1016/j.susc.2016.07.001.

References

[1] D.R. Mullins, P.M. Albrecht, F. Calaza, Variations in reactivity on different crystallographic orientations of cerium oxide, Top. Catal. 56 (2013) 1345–1362.
[2] A.D. McNaught, A. Wilkinson, A.D. Jenkins, IUPAC, Compendium of Chemical Terminology, 2nd ed. (the "Gold Book"). Blackwell Scientific Publications, Oxford, 1997 XML on-line corrected version: http://goldbook.iupac.org (2006-) created by M. Nic, J. Jirat, B. Kosata; updates compiled by A. Jenkins. ISBN 0-9678550-9-8. http://dx.doi.org/10.1351/goldbook.
[3] J.A. Dumesic, The Microkinetics of Heterogeneous Catalysis, American Chemical Society, 1993.
[4] P. Stoltze, Microkinetic simulation of catalytic reactions, Prog. Surf. Sci. 65 (2000) 65–150.
[5] A.A. Gokhale, S. Kandoi, J.P. Greeley, M. Mavrikakis, J.A. Dumesic, Molecular-level descriptions of surface chemistry in kinetic models using density functional theory, Chem. Eng. Sci. 59 (2004) 4679–4691.
[6] I. Chorkendorff, J.W. Niemantsverdriet, Concepts of Modern Catalysis and Kinetics, Wiley, 2007.
[7] O. Deutschmann, Modeling and Simulation of Heterogeneous Catalytic Reactions: From the Molecular Process to the Technical System, Wiley, 2013.
[8] A. Heyden, B. Peters, A.T. Bell, F.J. Keil, Comprehensive DFT study of nitrous oxide decomposition over Fe-Zsm-5, J. Phys. Chem. B 109 (2005) 1857–1873.
[9] J. Lu, A. Heyden, Theoretical investigation of the reaction mechanism of the hydrodeoxygenation of guaiacol over a Ru(0 0 0 1) model surface, J. Catal. 321 (2015) 39–50.
[10] J. Lu, S. Behtash, M. Faheem, A. Heyden, Microkinetic modeling of the decarboxylation and decarbonylation of propanoic acid over Pd(1 1 1) model surfaces based on parameters obtained from first principles, J. Catal. 305 (2013) 56–66.
[11] D. Chatterjee, O. Deutschmann, J. Warnatz, Detailed surface reaction mechanism in a three-way catalyst, Faraday Discuss. 119 (2002) 371–384.
[12] G. Krishnamurthy, A. Bhan, W.N. Delgass, Identity and chemical function of gallium species inferred from microkinetic modeling studies of propane aromatization over Ga/Hzsm-5 catalysts, J. Catal. 271 (2010) 370–385.
[13] A. Bhan, S.H. Hsu, G. Blau, J.M. Caruthers, V. Venkatasubramanian, W.N. Delgass, Microkinetic modeling of propane aromatization over Hzsm-5, J. Catal. 235 (2005) 35–51.
[14] G. Ellis, J. Sidaway, M.R.S. McCoustra, Numerical simulation of temperature-programmed reaction data: an application in surface chemical kinetics, J. Chem. Soc. Faraday Trans. 94 (1998) 2633–2637.
[15] C.-C. Wang, J.-Y. Wu, J.-C. Jiang, Microkinetic simulation of temperature-programmed desorption, J. Phys. Chem. C 117 (2013) 6136–6142.
[16] A. Heyden, A.T. Bell, F.J. Keil, Kinetic modeling of nitrous oxide decomposition on Fe-Zsm-5 based on parameters obtained from first-principles calculations, J. Catal. 233 (2005) 26–35.
[17] P. Budrugeac, Applicability of non-isothermal model-free predictions for assessment of conversion vs. time curves for complex processes in isothermal and quasi-isothermal conditions, Thermochim. Acta 558 (2013) 67–73.
[18] S. Tischer, O. Deutschmann, Recent advances in numerical modeling of catalytic monolith reactors, Catal. Today 105 (2005) 407–413.
[19] S. Katare, A. Bhan, J.M. Caruthers, W.N. Delgass, V. Venkatasubramanian, A hybrid genetic algorithm for efficient parameter estimation of large kinetic models, Comput. Chem. Eng. 28 (2004) 2569–2581.
[20] C. Dubien, D. Schweich, Three-way catalytic converter modelling. Numerical determination of kinetic data, in: A.F. N. Kruse, J.M. Bastin (Eds.), Studies in Surface Science and Catalysis, vol. 116, Elsevier 1998, pp. 399–408.
[21] R. Sanchirico, Model selection and parameters estimation in kinetic thermal evaluations using semiempirical models, AIChE J. 2012 (1869-1879) 58.
[22] G. Varhegyi, P. Szabo, E. Jakab, F. Till, Least squares criteria for the kinetic evaluation of thermoanalytical experiments. Examples from a char reactivity study, J. Anal. Appl. Pyrolysis 57 (2001) 203–222.
[23] R.S. Roche, Evaluation of kinetic parameters from TVA data. A computer simulation approach, J. Appl. Polym. Sci. 18 (1974) 3555–3569.
[24] E.S. Kurkina, N.L. Semendyaeva, A.I. Boronin, Mathematical modeling of nitrogen desorption from an iridium surface: a study of the effects of surface structure and subsurface oxygen, Kinet. Catal. 42 (2001) 703–717.
[25] M. Nele, E.L. Moreno, H.M.C. Andrade, Análise Estatística E Optimização De Perfis De Redução Termoprogramada (Tpr), Quim Nova 29 (2006) 641–645.
[26] J.A. Caballero, J.A. Conesa, Mathematical considerations for nonisothermal kinetics in thermal decomposition, J. Anal. Appl. Pyrolysis 73 (2005) 85–100.
[27] L.T. Biegler, J.J. Damiano, G.E. Blau, Nonlinear parameter-estimation - a case-study comparison, AICHE J. 32 (1986) 29–45.
[28] P. Bilardello, X. Joulia, J.M. Lelann, H. Delmas, B. Koehret, A general strategy for parameter-estimation in differential algebraic systems, Comput. Chem. Eng. 17 (1993) 517–525.
[29] J.E. Graciano, D.F. Mendoza, G.A.C. Le Roux, Performance comparison of parameter estimation techniques for unidentifiable models, Comput. Chem. Eng. 64 (2014) 24–40.
[30] G.D. Byrne, A.J. Degregoria, D.E. Salane, A program for fitting rate constants in gas-phase chemical-kinetics models, SIAM J. Sci. Stat. Comput. 5 (1984) 642–657.
[31] M. Shacham, N. Brauner, Application of stepwise regression for dynamic parameter estimation, Comput. Chem. Eng. 69 (2014) 26–38.
[32] K.A.P. McLean, K.B. McAuley, Mathematical modelling of chemical processes—obtaining the best model predictions and parameter estimates using identifiability and estimability procedures, Can. J. Chem. Eng. 90 (2012) 351–366.
[33] S. Vyazovkin, A.K. Burnham, J.M. Criado, L.A. Perez-Maqueda, C. Popescu, N. Sbirrazzuoli, ICTAC Kinetics Committee recommendations for performing kinetic computations on thermal analysis data, Thermochim. Acta 520 (2011) 1–19.
[34] M.I. Ortiz, A. Romero, A. Irabien, Integral kinetic-analysis from temperature programmed reaction data - alkaline-hydrolysis of ethyl-acetate as test reaction, Thermochim. Acta 141 (1989) 169–180.
[35] J.M. Bray, W.F. Schneider, First-principles analysis of structure sensitivity in no oxidation on Pt, ACS Catal. 5 (2015) 1087–1099.
[36] Y.K. Park, P. Aghalayam, D.G. Vlachos, A generalized approach for predicting coverage-dependent reaction parameters of complex surface reactions: application to H2 oxidation over platinum, J. Phys. Chem. A 103 (1999) 8101–8107.
[37] A. Savara, W. Ludwig, S. Schauermann, Kinetic evidence for a non-Langmuir-Hinshelwood surface reaction: H/D exchange over Pd nanoparticles and Pd (111), ChemPhysChem 2013 (1686-1695) 14.
[38] J.P. Clay, J.P. Greeley, F.H. Ribeiro, W. Nicholas Delgass, W.F. Schneider, DFT comparison of intrinsic WGS kinetics over Pd and Pt, J. Catal. 320 (2014) 106–117.
[39] C. Wu, D.J. Schmidt, C. Wolverton, W.F. Schneider, Accurate coverage-dependence incorporated into first-principles kinetic models: catalytic no oxidation on Pt (1 1 1), J. Catal. 286 (2012) 88–94.
[40] R.I. Masel, Principles of Adsorption and Reaction on Solid Surfaces, Wiley, New York, 1996 (p xiv, 804).
[41] J. Niemantsverdriet, K. Markert, K. Wandelt, The compensation effect and the manifestation of lateral interactions in thermal desorption spectroscopy, Appl. Surf. Sci. 31 (1988) 211–219.
[42] A.M. de Jong, J.W. Niemantsverdriet, Thermal desorption analysis: comparative test of ten commonly applied procedures, Surf. Sci. 233 (1990) 355–365.
[43] J.L. Falconer, J.A. Schwarz, Temperature-programmed desorption and reaction: applications to supported catalysts, Catal. Rev. Sci. Eng. 25 (1983) 141–227.
[44] M. Kislyuk, V. Rozanov, Temperature-programmed desorption and temperature-programmed reaction as methods for studying the kinetics and mechanism of heterogeneous catalytic processes, Kinet. Catal. 36 (1995) 80–88.
[45] J.J.M. Orfao, Review and evaluation of the approximations to the temperature integral, AICHE J. 53 (2007) 2905–2915.
[46] K. Koch, B. Hunger, O. Klepel, M. Heuchel, A new method of analysing temperature-programmed desorption (TPD) profiles using an extended integral equation, J. Catal. 172 (1997) 187–193.
[47] M.E. Brown, M. Maciejewski, S. Vyazovkin, R. Nomen, J. Sempere, A. Burnham, J. Opfermann, R. Strey, H.L. Anderson, A. Kemmler, R. Keuleers, J. Janssens, H.O. Desseyn, C.-R. Li, T.B. Tang, B. Roduit, J. Malek, T. Mitsuhashi, Computational aspects of kinetic analysis: part a: the ICTAC kinetics project-data, methods and results, Thermochim. Acta 355 (2000) 125–143.
[48] M. Maciejewski, Computational aspects of kinetic analysis.: part B: the ICTAC kinetics project — the decomposition kinetics of calcium carbonate revisited, or some tips on survival in the kinetic minefield, Thermochim. Acta 355 (2000) 145–154.
[49] B. Roduit, Computational aspects of kinetic analysis.: part E: the ICTAC kinetics project—numerical techniques and kinetics of solid state processes, Thermochim. Acta 355 (2000) 171–180.
[50] S. Vyazovkin, Computational aspects of kinetic analysis.: part C. The ICTAC kinetics project — the light at the end of the tunnel? Thermochim. Acta 355 (2000) 155–163.
[51] A. Savara, E. Weitz, Elucidation of intermediates and mechanisms in heterogeneous catalysis using infrared spectroscopy, Annu. Rev. Phys. Chem. 65 (2014) 249–273.
[52] D. Müller, E. Esche, López C, D. C.; Wozny, G. An algorithm for the identification and estimation of relevant parameters for optimization under uncertainty, Comput. Chem. Eng. 71 (2014) 94–103.
[53] A. Savara, Microkinetic Simulations of TPD of Methanol on CeO_2(111): Mechanistic Insights on H_2 and H_2O production, (submitted for publication) 2016.
[54] E. Ko, J. Benziger, R. Madix, Reactions of methanol on W (100) and W (100) — (5 × 1) C surfaces, J. Catal. 62 (1980) 264–274.
[55] E. Kautto, J. Kuhalainen, M. Manninen, Analysing methods for thermal desorption spectra, Phys. Scr. 55 (1997) 628–633.
[56] S. Vyazovkin, K. Chrissafis, M.L. Di Lorenzo, N. Koga, M. Pijolat, B. Roduit, N. Sbirrazzuoli, J.J. Sunol, ICTAC kinetics committee recommendations for collecting

experimental thermal analysis data for kinetic computations, Thermochim. Acta 590 (2014) 1–23.
[57] J.M. Criado, L.A. Pérez-Maqueda, Sample controlled thermal analysis and kinetics, J. Therm. Anal. Calorim. 80 (2005) 27–33.
[58] G. Varhegyi, Aims and methods in non-isothermal reaction kinetics, J. Anal. Appl. Pyrolysis 79 (2007) 278–288.
[59] N.M. Russell, J.G. Ekerdt, Nonlinear parameter estimation technique for kinetic analysis of thermal desorption data, Surf. Sci. 364 (1996) 199–218.
[60] V. Stuchly, Parametric sensitivity of complex temperature-programmed desorption, reaction and reduction, J. Therm. Anal. 35 (1989) 837–847.
[61] S.O. Vasquez, A new method for the analysis of heterogeneity using a modified temperature-programmed desorption technique, J. Chem. Soc. Faraday Trans. 88 (1992) 2051–2058.
[62] M.A. Deangelis, A.B. Anton, Temperature programming for isothermal desorption rate measurements, J. Vac. Sci. Technol. A 10 (1992) 3507–3516.
[63] P.J. Barrie, Analysis of temperature programmed desorption (TPD) data for the characterisation of catalysts containing a distribution of adsorption sites, Phys. Chem. Chem. Phys. 10 (2008) 1688–1696.
[64] P. Budrugeac, An iterative model-free method to determine the activation energy of heterogeneous processes under arbitrary temperature programs, Thermochim. Acta 523 (2011) 84–89.
[65] E.L. Haseltine, J.B. Rawlings, Approximate simulation of coupled fast and slow reactions for stochastic chemical kinetics, J. Chem. Phys. 117 (2002) 6959–6969.
[66] Z. Zlatev, Partitioning ODE systems with an application to air pollution models, Comput. Math. Appl. 42 (2001) 817–832.
[67] A. Sandu, D.N. Daescu, G.R. Carmichael, Direct and adjoint sensitivity analysis of chemical kinetic systems with KPP: part I—theory and software tools, Atmos. Environ. 37 (2003) 5083–5096.
[68] M. Celnik, R. Patterson, M. Kraft, W. Wagner, A predictor–corrector algorithm for the coupling of stiff ODEs to a particle population balance, J. Comput. Phys. 228 (2009) 2758–2769.
[69] R. Wolke, O. Knoth, Implicit–explicit Runge–Kutta methods applied to atmospheric chemistry-transport modelling, Environ. Model. Softw. 15 (2000) 711–719.
[70] J. Verwer, D. Simpson, Explicit methods for stiff ODEs from atmospheric chemistry, Appl. Numer. Math. 18 (1995) 413–430.
[71] A. Sandu, J. Verwer, M. Van Loon, G. Carmichael, F. Potra, D. Dabdub, J. Seinfeld, Benchmarking stiff ODE solvers for atmospheric chemistry problems-I. Implicit vs explicit, Atmos. Environ. 31 (1997) 3151–3166.
[72] A. Sandu, J. Verwer, J. Blom, E. Spee, G. Carmichael, F. Potra, Benchmarking stiff ODE solvers for atmospheric chemistry problems II: Rosenbrock solvers, Atmos. Environ. 31 (1997) 3459–3472.
[73] J. Verwer, Gauss-Seidel iteration for stiff ODEs from chemical kinetics, SIAM J. Sci. Comput. 15 (1994) 1243–1250.
[74] A.P.J. Jansen, An Introduction to Kinetic Monte Carlo Simulations of Surface Reactions, Springer, Berlin, Germany, 2012.
[75] Y. Cao, H. Li, L. Petzold, Efficient formulation of the stochastic simulation algorithm for chemically reacting systems, J. Chem. Phys. 121 (2004) 4059–4067.
[76] A. Slepoy, A.P. Thompson, S.J. Plimpton, A constant-time kinetic Monte Carlo algorithm for simulation of large biochemical reaction networks, J. Chem. Phys. (2008) (*128*, -.).
[77] J. Goutsias, Quasiequilibrium approximation of fast reaction kinetics in stochastic biochemical systems, J. Chem. Phys. 122 (2005) 184102.
[78] A. Samant, D.G. Vlachos, Overcoming stiffness in stochastic simulation stemming from partial equilibrium: a multiscale Monte Carlo algorithm, J. Chem. Phys. 123 (2005) 144114.
[79] Nist/Sematech E-Handbook of Statistical Methods, http://www.itl.nist.gov/div898/handbook/pmd/section4/pmd452.htm (accessed December 3, 2014).